Marine and Petroleum Geology 156 (2023) 106446

Contents lists available at ScienceDirect

Marine and Petroleum Geology

journal homepage: www.elsevier.com/locate/marpetgeo

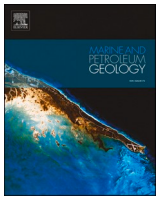

Spatial variations in diagenetic facies in tight sandstones from sublacustrine-fan deposits: Upper Triassic Yanchang formation, Ordos Basin, China

Wurong Wang [a,b], Dali Yue [a,b,*], Kenneth A. Eriksson [c], Shixiang Li [d], Yueyang Zhang [e], Jiarui Zhang [a,b], Zhen Li [d], Xiulin Hou [f], Wei Li [a,b], Hanqing Zhu [f], Shenghe Wu [a,b]

[a] National Key Laboratory of Petroleum Resources and Engineering, China University of Petroleum (Beijing), Beijing, 102249, China
[b] College of Geosciences, China University of Petroleum (Beijing), Beijing, 102249, China
[c] Department of Geosciences, Virginia Polytechnic Institute and State University, Blacksburg, VA, 24061, United States
[d] Research Institute of Petroleum Exploration & Development, PetroChina Changqing Oilfield Company, Xi'an, 710018, China
[e] Shale Oil Exploration and Development Headquarter, PetroChina Daqing Oilfield Company, Daqing, 163000, China
[f] Research Institute of Petroleum Exploration & Development, PetroChina, Beijing, 100083, China

ARTICLE INFO

Keywords:
Diagenetic facies
Spatial variation
Sublacustrine fan
Tight sandstone
Triassic Yanchang formation
Ordos Basin

ABSTRACT

Sublacustrine-fan, tight sandstones in the Yanchang Formation of the Ordos Basin are one of the most important tight-oil producing intervals in China and are reported here the key diagenetic facies. Five diagenetic facies are recognized in the Chang 6 tight sandstone interval, including relatively extensive dissolution (ED), relatively moderate dissolution with grain-coating illite (GCI), pore-filling illite cemented (PFI), extensive carbonate cemented (ECC), and tightly compacted (TC) diagenetic facies. A back-propagation (BP) neural network method is used to build an identification model of diagenetic facies in wells by correlating the various diagenetic facies with conventional well logs for which the identification accuracy can reach as high as 84.97%. Moreover, a novel method of interaction analyses of a large number of horizontal wells and small-spacing development wells and multidimensional constraints by the sedimentary architecture distribution is proposed to predict the distribution of diagenetic facies between wells, and a spatial variation model showing the stacking patterns and geometric features of diagenetic facies in tight sandstones from sublacustrine-fan deposits is established. Diagenetic facies varies more significantly in the direction perpendicular to the paleoflow than that in the direction parallel to paleoflow. The GCI diagenetic facies is most widely distributed within the lobe sandstone bodies as elongated lenses, usually irregularly surrounding the ED diagenetic facies or adjacent to PFI diagenetic facies. From the PFI, ED to GCI diagenetic facies, the average of width and length and the maximum thickness tend to increase. Furthermore, variations in thickness and proportion of various diagenetic facies are closely associated with lake-level cycles.

1. Introduction

Tight sandstone reservoirs have been extensively studied and commercially developed worldwide (e.g. Desbois et al., 2011; Zou et al., 2012; Caracciolo et al., 2015; Ghanizadeh et al., 2015; Critelli et al., 2018; Lai et al., 2018; Kadkhodaie et al., 2021; Ortiz-Orduz et al., 2021), such as the Alberta Basin in Canada (Masters, 1979; La Croix et al., 2013; Friesen et al., 2017), the Williston Basin, San Juan Basin and Appalachian basin in North America (Law, 2002; Hart, 2006; Ma et al., 2016), and the Ordos Basin, Songliao Basin, Junggar Basin, Sichuan Basin and Bohai Bay Basin in China (Xi et al., 2015; Yue et al., 2018; Zhu et al., 2019; Li et al., 2022a; Jiang et al., 2023). Diagenetic facies, which is a comprehensive description of diagenetic minerals and the type and intensity of diagenesis, determines the variation of reservoir quality in tight sandstones (Higgs et al., 2007; Zou et al., 2008; Barbera et al., 2011; Ozkan et al., 2011; Cui et al., 2017; Lai et al., 2018). Compared to marine deep-water reservoirs, tight sandstone reservoirs composed of lacustrine, deep-water sediments have greater variability in composition and more complex lithofacies (Stevenson and Peakall, 2010; Amendola et al., 2016; Liu et al., 2017, 2020; Bell et al., 2018; Yang et al., 2018),

* Corresponding author. National Key Laboratory of Petroleum Resources and Engineering, China University of Petroleum (Beijing), Beijing, 102249, China.
E-mail address: yuedali@cup.edu.cn (D. Yue).

https://doi.org/10.1016/j.marpetgeo.2023.106446
Received 16 May 2023; Received in revised form 3 August 2023; Accepted 3 August 2023
Available online 4 August 2023

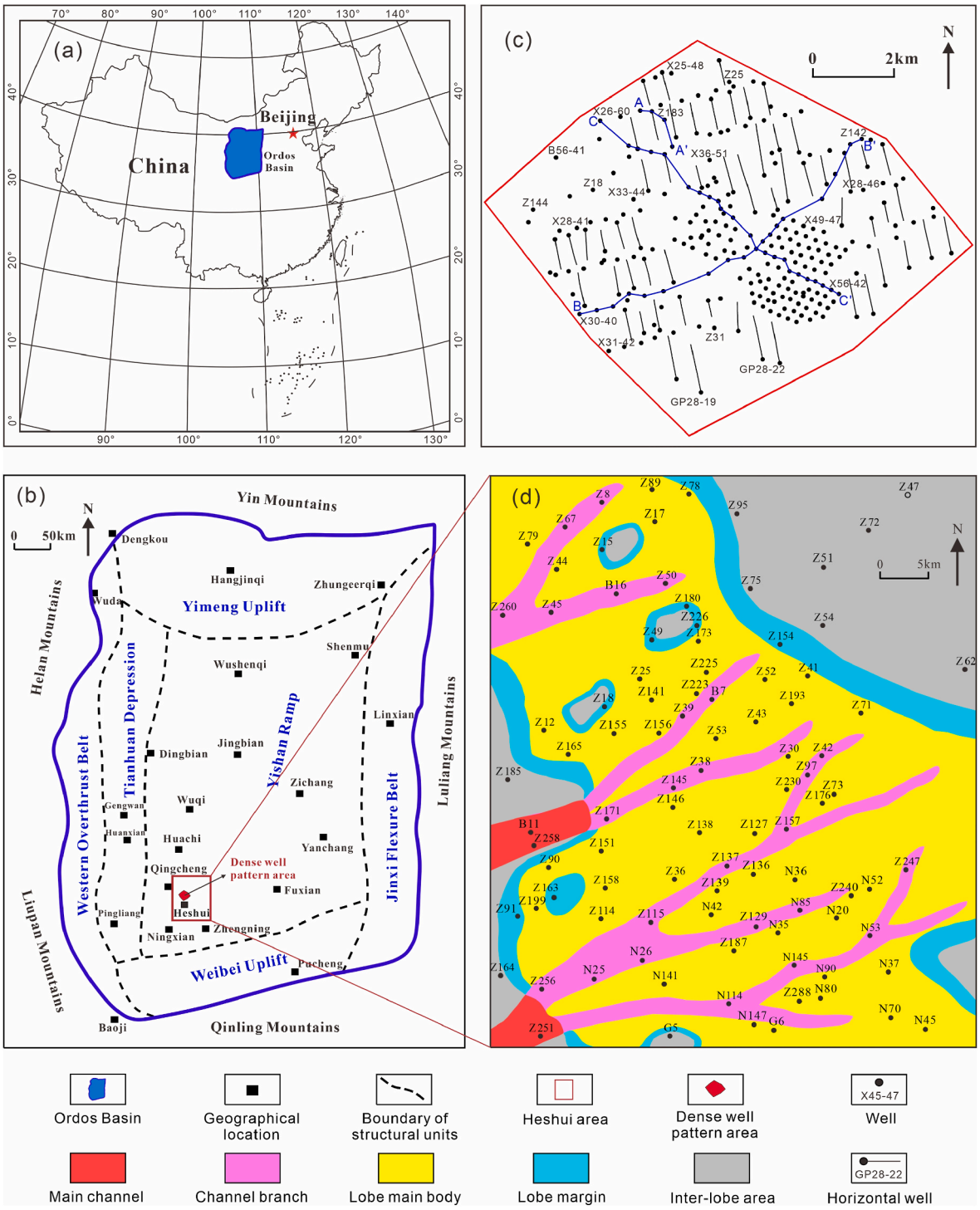

Fig. 1. Geological setting of the study area. (a) Map of China showing the location of the Ordos Basin (modified after Lai et al., 2016; Wang et al., 2020a); (b) Tectonic subdivisions of the Ordos Basin and location of the study area (modified after Wang et al., 2020a); (c) Area with dense well pattern showing well locations; (d) Sedimentary facies distribution of the Chang 6_2 interval (modified after Wang et al., 2019).

which makes the prediction of diagenetic facies in tight sandstones within sublacustrine-fan deposits much more difficult, but of great significance for tight oil development.

Cores and corresponding thin section observations and scanning electron microscope (SEM) analyses are the most effective means to identify various diagenetic facies (Morad et al., 2010; Nguyen et al., 2013; Higgs et al., 2017; Wu et al., 2020; Li et al., 2022b). Recent studies have correlated diagenetic facies with conventional well logs to perform diagenetic facies prediction via a set of log responses in tight sandstones (Ozkan et al., 2011; Ran et al., 2016; Cui et al., 2017; Wu et al., 2020; Zhao et al., 2022), so as to overcome the problem of a lack of cores and reduce cost of core experiments. Interdisciplinary approaches have been proposed to predict diagenetic facies by building prediction models using different statistic algorithms, such as the principal component analysis (PCA) (Cui et al., 2017; Li et al., 2022b), hierarchical cluster analysis (HCA) (Li et al., 2019; Zhao et al., 2022), linear discriminant analysis (LDA) (Wang et al., 2017a), and artificial neural networks (Wang and Lu, 2021). Artificial neural network algorithms are generally

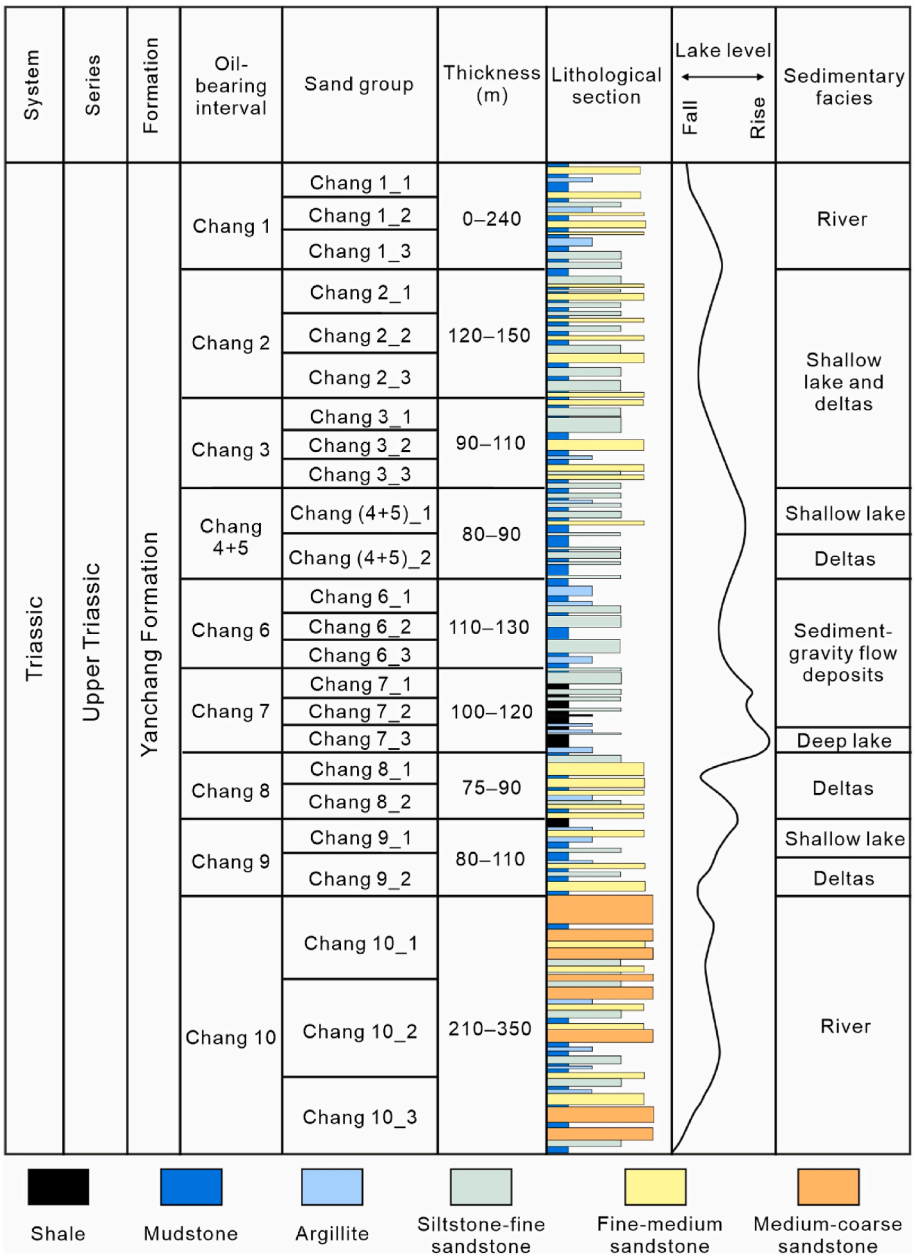

Fig. 2. Stratigraphic section and sedimentary facies of the Upper Triassic Yanchang Formation in the Ordos Basin (modified after Yao et al., 2018).

considered to be capable of greatly improving efficiency and possibly the accurate identification of diagenetic facies (Li et al., 2021, 2022b; Wang and Lu, 2021). However, it should be noted that previous research efforts for the prediction of diagenetic facies were mainly focused on single wells (Lai et al., 2018; Wu et al., 2020), while spatial variations of diagenetic facies in tight sandstones are still poorly understood.

Diagenetic alterations and the spatial distribution of diagenetic facies are controlled by the complex sedimentary architecture (including architecture element types, scales, geometries, and stacking patterns) (Dutton, 2008; Morad et al., 2010; Wu, 2010; Fu et al., 2013; Wang et al., 2022a), resulting in significant variations of reservoir quality. Previous studies have discussed the distribution characteristics of diagenetic alterations and reservoir quality linked to sedimentary facies, such as fluvial, deltaic, and deep-water deposits (Morad et al., 2000; Dill et al., 2005; El-Ghali et al., 2006; Li et al., 2017; Wang et al., 2019), but spatial distribution models of diagenetic facies under the constraints of sedimentary architecture is still confusing, especially in lacustrine deep-water tight sandstone reservoirs. Some scholars have proposed to illustrate the plane or profile distribution of diagenetic facies by correlating seismic data with core-derived diagenetic facies (Zeng et al., 2018; Zhang et al., 2018, 2019; Zhu et al., 2020; Wang et al., 2022a, 2022b), but due to limitations of the resolution of seismic data, or even a lack of seismic data, prediction of diagenetic facies distribution between wells in thin intervals remains challenging. A few previous studies have interpreted the planar distribution of dominant diagenetic facies under the control of sand body boundaries obtained from multi-well data (Ma et al., 2018; Cao et al., 2021; Yu et al., 2022). However, previous studies have always ignored the controlling effect of different sedimentary architecture elements on the types and distribution of various diagenetic facies, especially for tight sandstones within sublacustrine-fan deposits. Furthermore, the lateral extent of different diagenetic facies in horizontal wells is rarely documented and, as a result, the spatial variation of reservoir quality is still not adequately constrained. The quantitative scale, geometry and spatial stacking patterns of different diagenetic facies within sublacustrine-fan deposits remain to be clarified.

The main purpose of this study is to explore spatial variations in

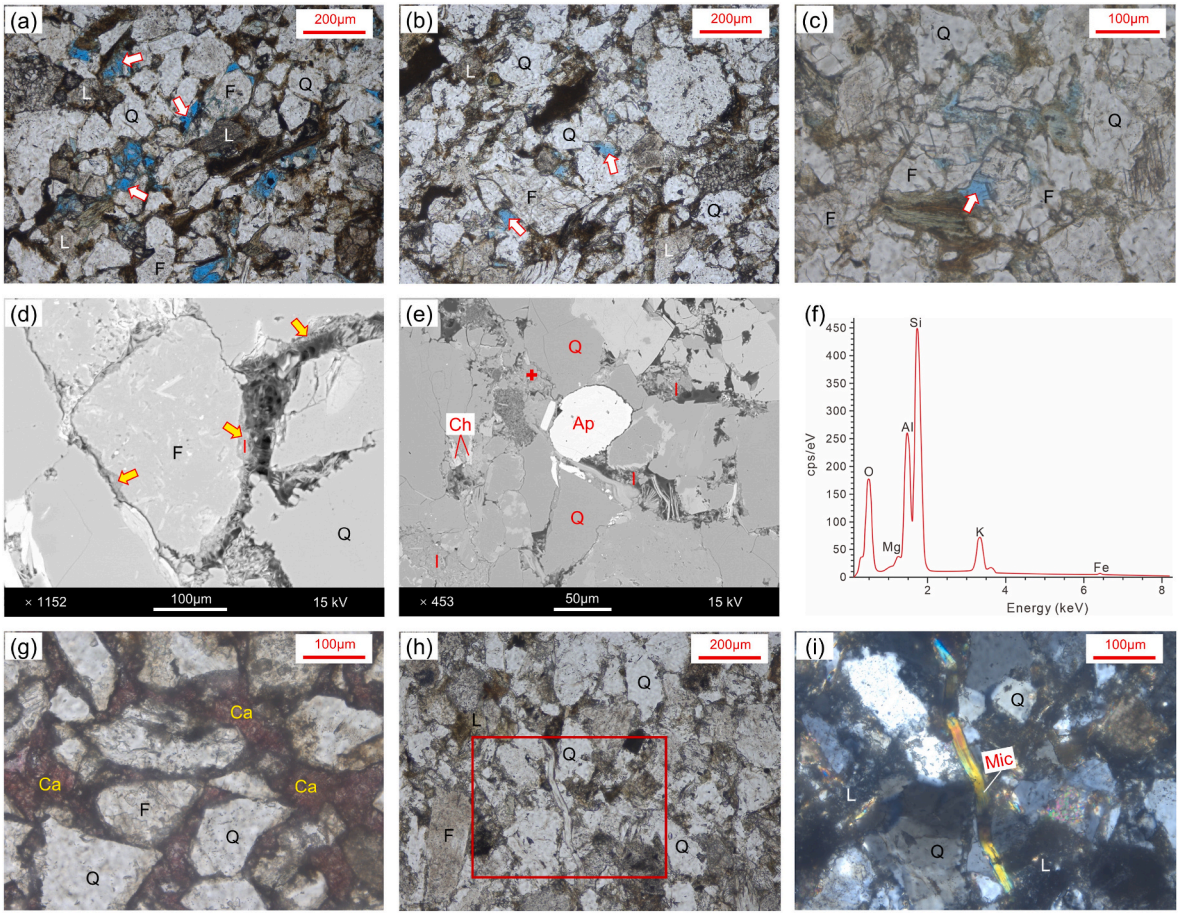

Fig. 3. Diagenetic characteristics of various diagenetic facies in the Chang 6 tight sandstones. (a) ED diagenetic facies (PPL image; Well Z199, 1505.2 m; Φ = 8.16%, K = 0.11 mD); (b) GCI diagenetic facies (PPL image; Well Z127, 1528.3m; Φ = 7.29%, K = 0.047 mD); (c) and (d) PPL and BSE showing GCI diagenetic facies (Well Z115, 1571.94m; Φ = 8.19%, K = 0.078 mD); (e) PFI diagenetic facies (BSE image; Well Z127, 1479.2m; Φ = 6.4%, K = 0.029 mD); (f) EDS spectrum of the authigenic illite marked by the red cross in (e); (g) ECC diagenetic facies (PPL image; Well N25, 1408.45m; Φ = 1.16%, K = 0.002 mD); (h) TC diagenetic facies (PPL image; Well Z127, 1483.65m; Φ = 2.66%, K = 0.006 mD); (i) Magnified XPL image of the pane in (h). Q = quartz; F = feldspar; L = lithic fragments; Ca = carbonate cement; Ap = apatite; I = illite; Ch = chlorite; Mic = mica; XPL = cross-polarized light; PPL = plane-polarized light; BSE = backscattered electron; EDS = energy dispersive spectrometer; Φ = helium porosity; K = nitrogen permeability; White-filled arrows indicate intergranular pores and dissolution pores; Yellow-filled arrows indicate grain-coating illite.

diagenetic facies of tight sandstones within sublacustrine-fan deposits of the Upper Triassic Yanchang Formation, Ordos Basin. By integrating thin section observations, SEM and X-ray diffraction (XRD) analysis, a classification is proposed for diagenetic facies in the tight sandstones, and the intelligent prediction of diagenetic facies using back-propagation (BP) neural network was addressed in wells or in intervals without core data. Furthermore, the spatial distribution of sandstone diagenetic facies within a sedimentary architecture framework was carefully investigated by combining a large number of horizontal wells and development wells with close spacing to generate a three-dimensional model showing the spatial variation in diagenetic facies of tight sandstones within sublacustrine-fan deposits. This interdisciplinary study can provide new insights into the prediction of diagenetic facies distribution and reservoir quality evaluation in lacustrine deep-water tight sandstone reservoirs.

2. Geological setting

The Ordos Basin is the second largest sedimentary basin in central China (Fig. 1a), with an area of approximately 2.6×10^5 km^2. The Ordos Basin experienced a series of complex tectonic processes from the Mesoproterozoic to the Quaternary (Yang, 2002). During the late Triassic, the Ordos Basin was transformed from a marine basin into an intracratonic basin due to the collision of the North China Plate with the Yangtze Plate (Yang et al., 2014; Wang et al., 2017b), leading to the formation of the fluvial to lacustrine depositional system (Fig. 2). The study area, the Heshui area, is located in the southwestern corner of the Yishan Ramp of the Ordos Basin (Fig. 1b). A typical well distribution area in the middle of the Heshui area consists of 276 wells (58 horizontal wells) with an average well spacing of approximately 250 m (Fig. 1c).

The Upper Triassic Yanchang Formation is composed of Chang 10 to Chang 1 oil-bearing intervals from bottom to top (Fig. 2) (Yao et al., 2018). The Chang 6 oil-bearing interval, the focus of this study, can be subdivided into three units, namely Chang 6_1, Chang 6_2, and Chang 6_3 (Fig. 2). Moreover, the Chang 6_3 interval can be divided into three thin intervals (Chang 6_3_3, Chang 6_3_2 and Chang 6_3_1, with an average thickness of 17 m, 19 m and 12 m, respectively) from bottom to top, and the Chang 6_2 can be divided into two thin intervals (Chang 6_2_2 and Chang 6_2_1, with an average thickness of 20 m and 22 m, respectively) (Qu et al., 2021). Sublacustrine-fan sedimentary facies is widely developed in the Chang 6 interval of the Hehsui area (Figs. 1d and 2) (Wang et al., 2019; Qu et al., 2021), and sedimentary architecture units such as main channel, channel branch, lobe main body and lobe margin are developed from proximal to distal parts of the fan (Fig. 1d). Lithologies in the Chang 6 interval are dominated by fine-grained sandstone, siltstone and dark grey to black mudstone. Various

Table 1
Characteristics of various diagenetic facies in the Chang 6 tight sandstones.

Diagenetic facies	Major lithofacies (modified after Wang et al., 2019)	Diagenetic sequence (modified after Wang et al., 2019)		Diagenetic facies code
		Eodiagenesis	Mesodiagenesis	
Relatively extensive dissolution diagenetic facies	Fine-grained, cross-bedded sandstones (Sc)	Limited mechanical compaction, limited feldspar dissolution and carbonate cementation	Relatively extensive dissolution, limited carbonate cementation and compaction	ED
Relatively moderate dissolution with grain-coating illite diagenetic facies	Fine-grained, massive-bedded sandstones (Sm)	Moderate mechanical compaction, limited carbonate cementation and dissolution	Relatively moderate dissolution, grain-coating illite cementation, limited carbonate cementation, and moderate compaction	GCI
Pore-filling illite cemented diagenetic facies		Moderate mechanical compaction, grain-coating illite cementation, limited carbonate cementation and dissolution	Abundant pore-filling illite cementation, moderate compaction, and relatively weak dissolution	PFI
Extensive carbonate cemented diagenetic facies	Fine-grained, cross-bedded sandstones (Sc) or fine-grained, massive-bedded sandstones (Sm)	Limited mechanical compaction, partial to extensive early carbonate cementation	Extensive carbonate cementation, limited mechanical compaction and dissolution	ECC
Tightly compacted diagenetic facies	Siltstone to very fine-grained sandstones (Ss)	Extensive mechanical compaction	Extensive mechanical compaction, limited dissolution and cementation	TC

lithofacies have been identified in the Chang 6 sandstones (Wang et al., 2019), including fine-grained, cross-bedded sandstone (Sc), fine-grained, massive-bedded sandstone (Sm), and siltstone to very fine-grained sandstone (Ss). The porosity of the Chang 6 sandstones mainly ranges from 1% to 13% with an average of 8%, and the permeability is mainly 0.001–0.65 mD with an average of 0.09 mD, typical of tight sandstones.

3. Dataset and methods

The types of diagenetic facies in the Chang 6 tight sandstones are identified based on analyses of petrographic characteristics, pore types, diagenetic minerals, intensity of diagenesis and diagenetic sequences obtained from various core experiments, including impregnated thin section analysis of 324 samples, SEM observations with secondary electron (SE) imaging of 157 samples, SEM observations with back-scattered electron (BSE) imaging of 4 representative samples, XRD analysis of 31 representative samples, and helium porosity and nitrogen permeability measurements of 189 samples. The suite of conventional well logs run in the Heshui area mainly consist of gamma ray (GR), caliper (CAL), acoustic transit time (AC), spontaneous potential (SP), true formation resistivity (RT) and bulk density (DEN).

Variations in diagenetic facies between wells in thin intervals are investigated using a novel method of interaction analyses of a large number of horizontal wells and small-spacing development wells and multidimensional constraints by the sedimentary architecture

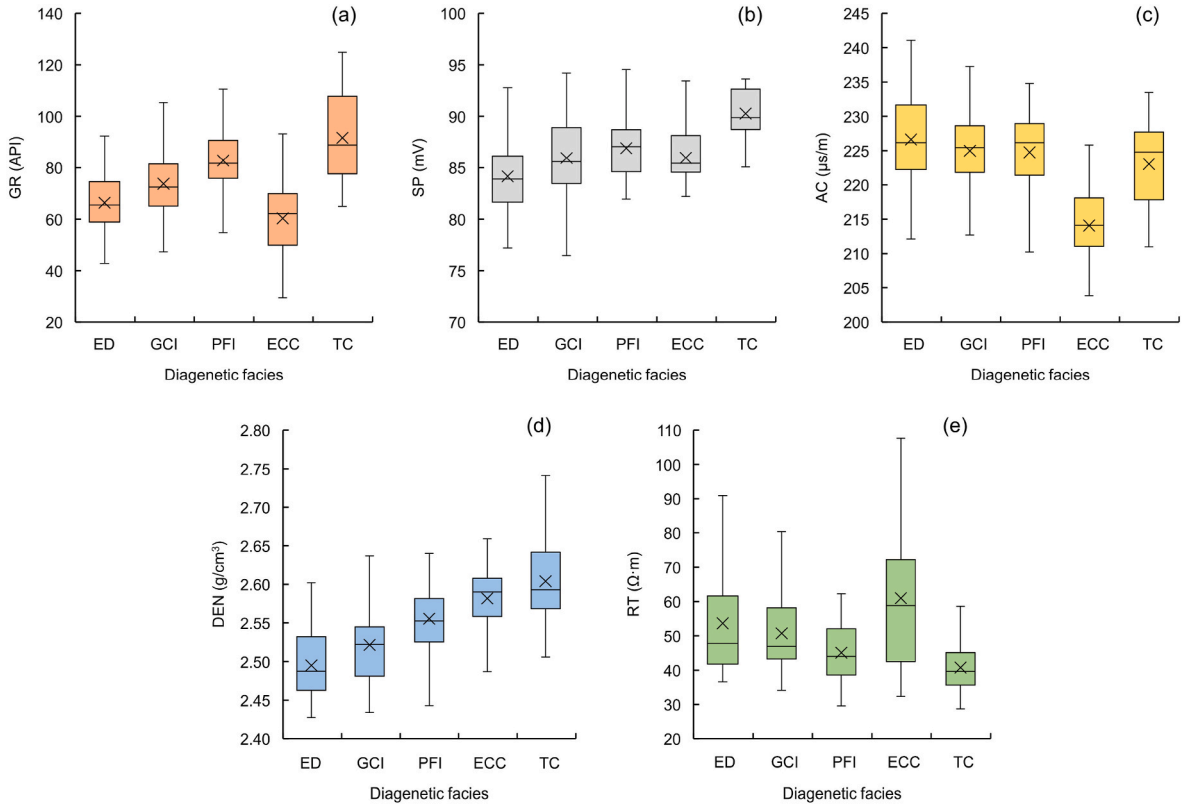

Fig. 4. Variation ranges of well-log responses for the five diagenetic facies in the Chang 6 tight sandstones. (a) Gamma ray (GR); (b) Spontaneous potential (SP); (c) Acoustic transit time (AC); (d) Bulk density (DEN); (e) True formation resistivity (RT). The descriptions of the diagenetic facies codes ED, GCI, PFI, ECC and TC are shown in Table 1.

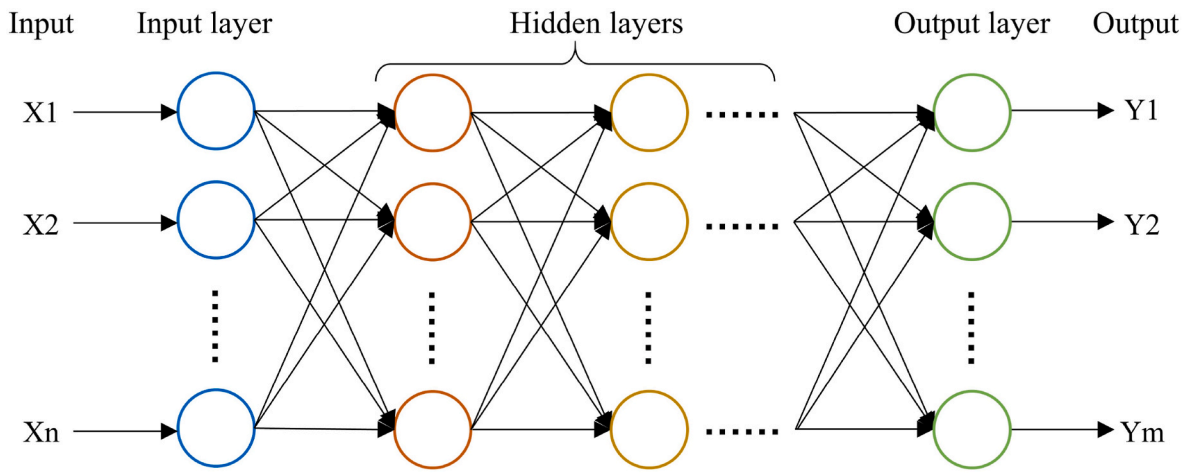

Fig. 5. Topological structure of BP neural network including input layers, hidden layers and output layers (modified after Wang et al., 2013).

distribution, including vertical constraints of the thin-interval stratigraphic framework, lateral constraints of the sedimentary architecture distribution of single sand bodies, and quantitative scale constraints from a large number of the horizontal wells. This study assumes that the spatial distribution of diagenetic facies is significantly controlled by a complex sedimentary architecture (Morad et al., 2010; Wu, 2010; Fu et al., 2013). Single-well interpretations of sedimentary architectural elements (main channel, channel branch, lobe main body, lobe margin and inter-lobe area) and the sedimentary architecture in the study area have been carefully investigated in previous studies (Fig. 1d) (e.g. Wang et al., 2019; Qu et al., 2021).

4. Results

4.1. Diagenetic facies types and log responses

4.1.1. Diagenetic facies types and characteristics

Diagenetic alterations and diagenetic minerals vary between different diagenetic facies (Lai et al., 2018). The dominant diagenetic characteristics in the Chang 6 tight sandstones of the Heshui area include mechanical compaction, feldspar dissolution, and precipitation of carbonate cements and abundant illite cements (16%–72% of the total clay minerals, with an average of 49%) (Wang et al., 2019). Thin section analysis, SEM, XRD, and fluid inclusion analysis have identified different diagenetic evolution processes in the Chang 6 tight sandstones of the Heshui area (Wang et al., 2019), resulting in various diagenetic facies (Fig. 3), including relatively extensive dissolution (ED), relatively moderate dissolution with grain-coating illite (GCI), pore-filling illite cemented (PFI), extensive carbonate cemented (ECC), and tightly compacted (TC) diagenetic facies. Different lithofacies usually show different diagenetic facies, and the same lithofacies can also display different diagenetic facies due to the quite different diagenetic processes. Typical diagenetic characteristics and petrophysical properties for each type of diagenetic facies are illustrated in Table 1. The ED diagenetic facies with relatively extensive dissolution and limited carbonate cementation commonly exhibits the best reservoir quality, whereas the ECC with extensive carbonate cementation and the TC diagenetic facies with extensive mechanical compaction show the worst reservoir quality (Wang et al., 2019).

4.1.2. Log responses of various diagenetic facies

Conventional well logs are a record of lithofacies, pore structure and diagenetic features (Lai et al., 2018, 2020), and therefore logging values can reflect the characteristics of diagenetic facies. By investigating well log responses of various diagenetic facies in cored wells, well logs sensitive to variations in diagenetic minerals can be used to predict

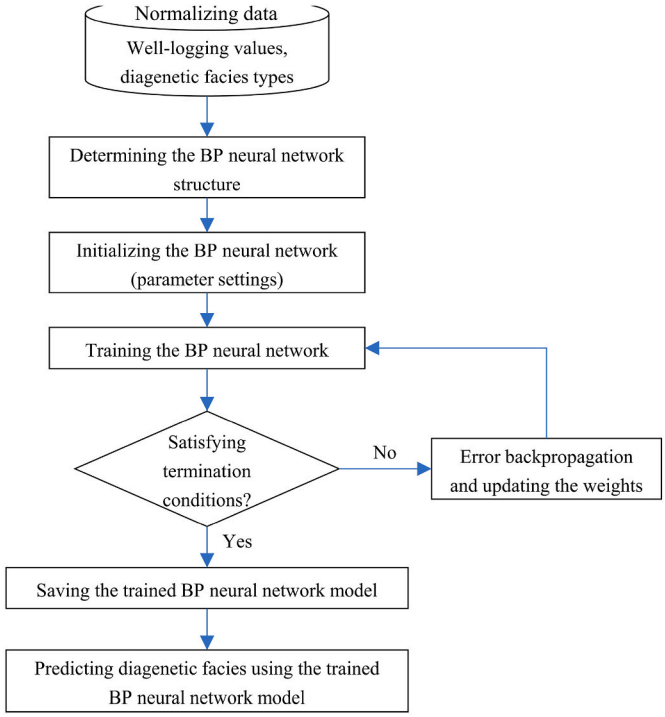

Fig. 6. Flowchart of how to predict diagenetic facies based on the BP neural network algorithm in this study.

diagenetic facies in wells or intervals without core data. It should be noted that prior to collecting logging values for various diagenetic facies, core-to-log depth matching was performed and the well logs were standardized using multi-well histogram and cross-plot displays (Salim et al., 2017). As can be seen from Fig. 4, the well log curves sensitive to the types of diagenetic facies in the Chang 6 sandstones include gamma ray (GR), spontaneous potential (SP), acoustic transit time (AC), bulk density (DEN), and true formation resistivity (RT), especially AC, DEN and GR logs. Variation ranges of well-log responses for the five diagenetic facies in the Chang 6 tight sandstones are summarized in Fig. 4. ECC diagenetic facies are easily recognized on well logs by the lowest GR and AC values due to the presence of a large amounts of carbonate cement. Except ECC diagenetic facies, GR, DEN and SP values gradually increase from ED to GCI to PFI to TC diagenetic facies, while AC and RT values show the opposite trend.

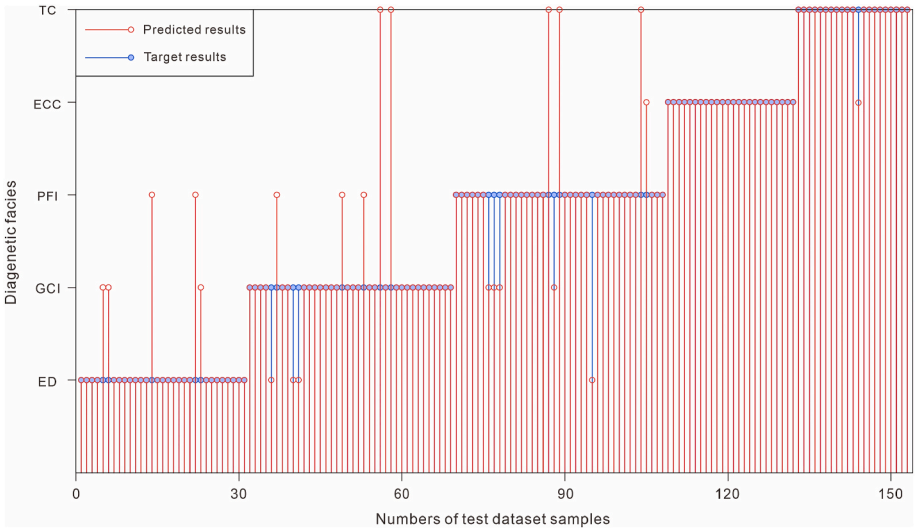

Fig. 7. Logging identification results of diagenetic facies using the BP neural network method on the test dataset. The descriptions of the diagenetic facies codes ED, GCI, PFI, ECC and TC are shown in Table 1.

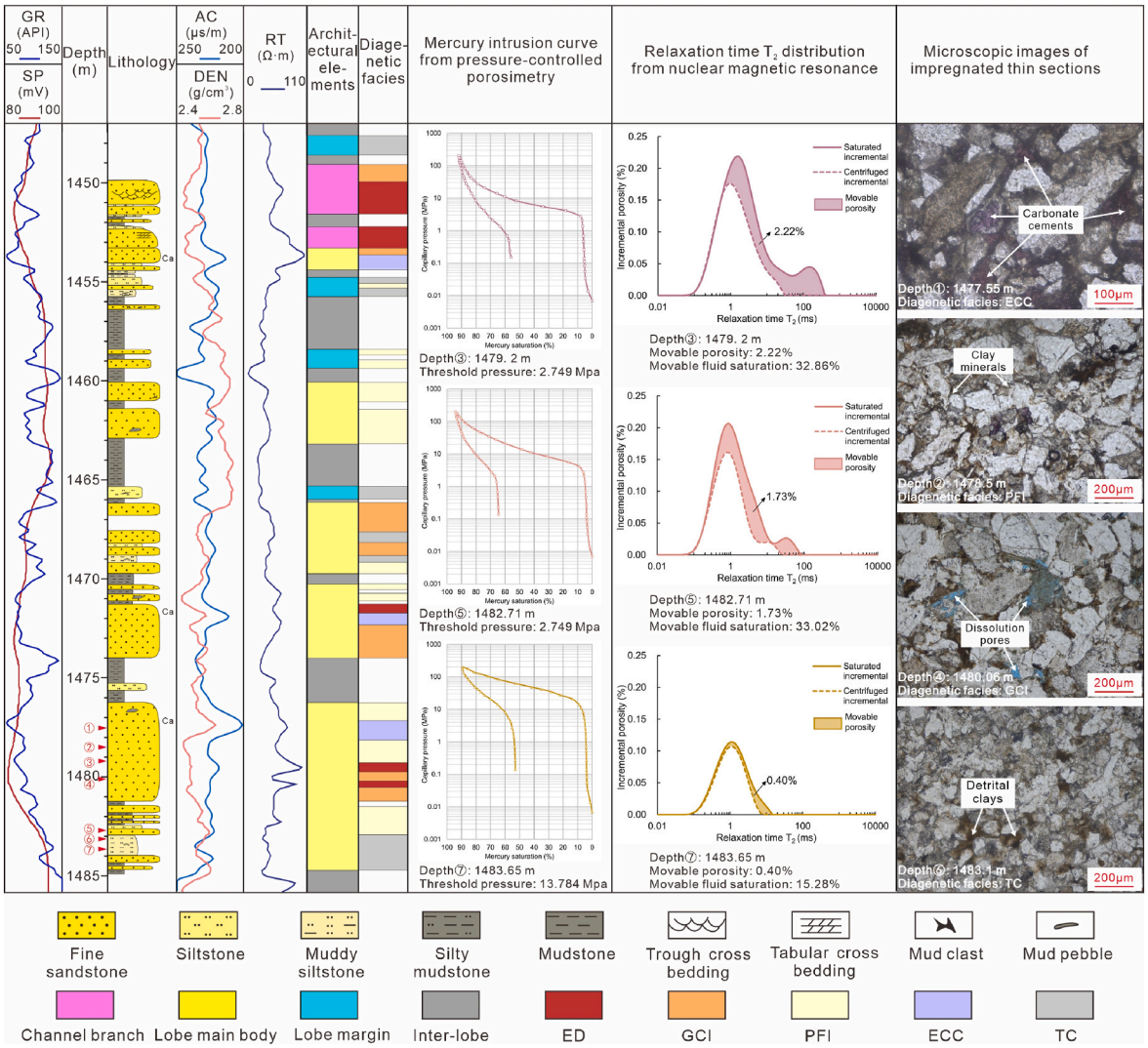

Fig. 8. Logging identification results of diagenetic facies of Chang 6 tight sandstones in Well Z127, as well as the mercury intrusion curves from PCP, relaxation time T_2 distribution from NMR, and microscopic images of impregnated thin sections for various diagenetic facies. The PCP samples are quoted from Wang et al. (2020b); the NMR samples are quoted from Wang et al. (2020a); the lithology and sedimentary architectural element columns are modified from Wang et al. (2019).

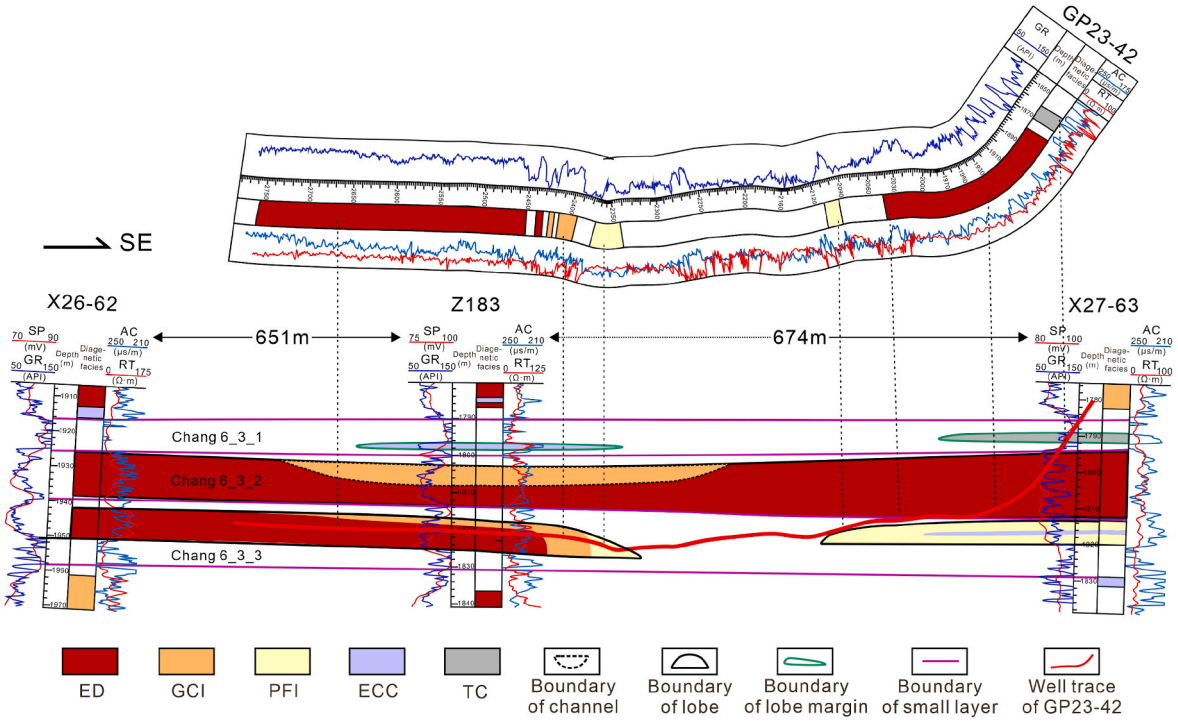

Fig. 9. Profile distribution of diagenetic facies in the Chang 6 tight sandstones within the framework of sedimentary architecture correlation (see AA' in Fig. 1c for the section location). The boundary of the lobe limits the distribution of the composite sand body of the lobe main body and the lobe margin.

4.2. Well-log identification of diagenetic facies using BP neural network

The back-propagation (BP) neural network has long been regarded as an effective method for solving complex nonlinear geological problems (Qiu et al., 2001; Gogoi and Chatterjee, 2019; Lu et al., 2021). The topological structure of the BP neural network including the input layer, hidden layer and output layer is shown in Fig. 5 (Wang et al., 2013). To achieve a high-accuracy prediction of diagenetic facies in this work, the BP neural network was established on MATLAB software to pursue the nonlinear mapping relationship between the logging responses (input layer) and the types of diagenetic facies (output layer). Specifically, the input layer consists of the normalized logging data pairs with GR, SP, AC, DEN and RT values, and the output layer contains the five types of identified diagenetic facies, namely ED, GCI, PFI, ECC and TC. The implementation process of predicting diagenetic facies based on the BP neural network algorithm are shown in Fig. 6.

4.2.1. Accuracy of identification of diagenetic facies

To examine the accuracy of diagenetic facies identification using the BP neural network, 70% of samples (356 samples) with thin sections or SEM images were selected as the training dataset to build the nonlinear mapping relationship between logging values and diagenetic facies, and the remaining 30% of samples (153 samples) were utilized as a test dataset. The maximum number of iterations on the training dataset was set to 3000 and training error of prediction values relative to the real value was within 0.025 until the iteration was complete. Logging identification results on the test dataset show that ECC diagenetic facies were all correctly identified, and only one case of TC diagenetic facies was misidentified as ECC diagenetic facies (Fig. 7). ED diagenetic facies has an identification accuracy of 83.87%, with 5 cases of misidentification (Fig. 7). GCI diagenetic facies and PFI diagenetic facies have relatively low identification accuracy, with 8 and 9 misidentified cases, respectively (Fig. 7). On the whole, the identification accuracy of the diagenetic facies using the BP neural network method is as high as 84.97%, which is sufficient to meet the actual demand of petroleum exploration and development (Li et al., 2022b).

4.2.2. Validation of high consistency of diagenetic facies identified by BP neural network with core analysis results

A blind test was carried out to evaluate the validation of the trained BP neural network model in Well Z127 that did not participate in the model construction. Fig. 8 shows that the well-log identification results of diagenetic facies at depths of 1477.55 m, 1478.5 m, 1480.06 m, and 1483.1 m are consistent with the recognition results using impregnated thin sections at the corresponding depths. Due to strong mechanical compaction of the TC diagenetic facies, the pore connectivity of sandstones with this diagenetic facies is significantly worse than that of sandstones of the PFI diagenetic facies. Mercury intrusion curves from pressure-controlled porosimetry (PCP) and relaxation time T_2 distributions from nuclear magnetic resonance (NMR) show that the TC diagenetic facies identified at a depth of 1483.65 m have poorer pore connectivity and lower movable fluid content than the PFI diagenetic facies identified at depths of 1479.2 m and 1482.71 m (Fig. 8), which also verifies the reliability of the well-logging identification results. Considering the prediction results and the analysis results by thin section of the PCP and NMR samples, the types of diagenetic facies predicted by the trained BP neural network model has a high degree of consistency with the core experimental analysis results (Fig. 8), suggesting that the trained BP neural network model can be effectively applied to predict diagenetic facies of the Chang 6 sandstones in the Heshui area.

5. Discussion

5.1. Stacking patterns and geometric features of diagenetic facies for the Chang 6 tight sandstones

5.1.1. Diagenetic facies variations in horizontal wells as a guide for the prediction of inter-well diagenetic facies correlation

Prior to investigating the correlation of diagenetic facies between wells, the types of diagenetic facies in individual wells were identified using conventional well logs based on the BP neural network method discussed in Section 4.2. In this study, the approach of integrating

Table 2
Maximum lateral extent of different diagenetic facies of the Chang 6 tight sandstones in the horizontal section of horizontal wells located in the dense well pattern area.

Well	Maximum lateral extent (m)					Well	Maximum lateral extent (m)				
	ED	GCI	PFI	ECC	TC		ED	GCI	PFI	ECC	TC
GP22-20	194.9	46.7	0	8.9	32.3	GP25-23	242.5	104.4	86.6	5.7	5.2
GP22-21	16.9	244.4	63.5	0	0	GP25-24	204.8	232.3	34.3	5.3	13.5
GP22-211	81	384.6	290.6	18.1	33.9	GP25-25	210.5	48.1	58.7	0	14.3
GP22-42	275.1	144.6	56.3	0	50.9	GP25-26	241.8	214.7	101.4	0	19.1
GP22-43	94.8	314.4	165.3	5.5	23.4	GP26-14	154.4	142.6	66.3	10.6	162
GP22-46	273.5	120.2	127.6	0	0	GP26-16	119.7	144.6	90.3	11	42.5
GP23-22	153.9	214.1	67.3	3.3	10.2	GP26-17	162.3	88	46.6	24.4	19.2
GP23-41	422.6	311.7	0	0	0	GP26-18	254.7	71.7	78.1	0	79.2
GP23-42	302.8	18.7	24.3	0	0	GP26-19	135.2	223.8	48	26.5	108.2
GP23-43	128.7	313	63.1	0	16.9	GP26-22	235.6	189.7	64.6	6.6	20.1
GP23-44	534.8	32.7	9.5	0	15.5	GP26-241	113.8	57.2	115.6	5	22.7
GP23-45	281.1	139.1	60	6.4	11.6	GP26-25	164.8	54.8	52.1	2.6	62.7
GP23-46	175.3	264.6	101.4	7.9	17.4	GP26-26	396.5	178.4	164.9	8.4	11.3
GP24-21	144.6	146.1	97.8	4.5	19.8	GP27-16	713	44.8	0	2.3	4.1
GP24-22	88.2	54	32.4	10.6	29.3	GP27-17A	204.8	0	78.8	8.6	11.7
GP24-23	684.3	135.5	148.9	0	14.9	GP27-18	123	172.8	255.2	0	19.9
GP24-24	178.4	199.5	343.6	18.7	100.4	GP27-19	224.9	219.7	137.2	15.2	70.7
GP24-41	249	144.1	28.6	0	7.5	GP27-20	246.8	0	89	0	7.6
GP24-42	226.9	415.4	0	4.7	0	GP27-21	108.2	232.3	345.9	17.2	22.6
GP25-13	286.2	83	100.1	3.5	42.3	GP27-22	122.3	302.8	77.4	2.4	56.6
GP25-14	242.3	37.9	76.4	7.8	27.1	GP27-23	174.5	392.6	56.6	10.1	122.1
GP25-15	523.8	19	0	2	18.6	GP27-24	364.7	117.1	56.5	18.8	114.1
GP25-16	58.7	207.4	169.1	7.7	20.3	GP27-26	504.6	209.3	55.4	1.8	22.8
GP25-17	643.4	0	0	3.5	0	GP27-27	570.3	232.1	0	28.1	29.8
GP25-18	204.1	56.5	65.2	3.4	14.2	GP27-28	249.1	108.2	113.3	0	19.8
GP25-19	177.6	46.9	30.6	11	7.9	GP28-18	722	43.4	35.2	5.1	7.1
GP25-20	207.9	74.3	16.2	2.1	19.6	GP28-19	465.6	217.7	122.1	5	21.9
GP25-21	248.7	280.5	103.3	11.3	83.9	GP28-22	139.3	146.5	108.4	11.2	14.1
GP25-22	85.8	228.8	65.7	0	44.5	GP28-23	215.5	373.4	203.9	8.6	19

multidimensional constraints by the sedimentary architecture distribution with interaction analyses of a large number of horizontal wells and small-spacing development wells is proposed to predict the distribution of diagenetic facies between wells. As shown in the correlation well section in Fig. 9, combined with the sedimentary architecture distribution (channel branch, lobe main body and lobe margin) and the distribution of different diagenetic facies identified in the horizon well GP23-42, the distribution of diagenetic facies between wells X26-62 and X27-63 is illustrated under the constraint of sedimentary architecture distribution. The interaction analyses of a total of 58 horizontal wells and 218 development wells with small spacing were conducted to determine the inter-well diagenetic facies distribution in the dense well

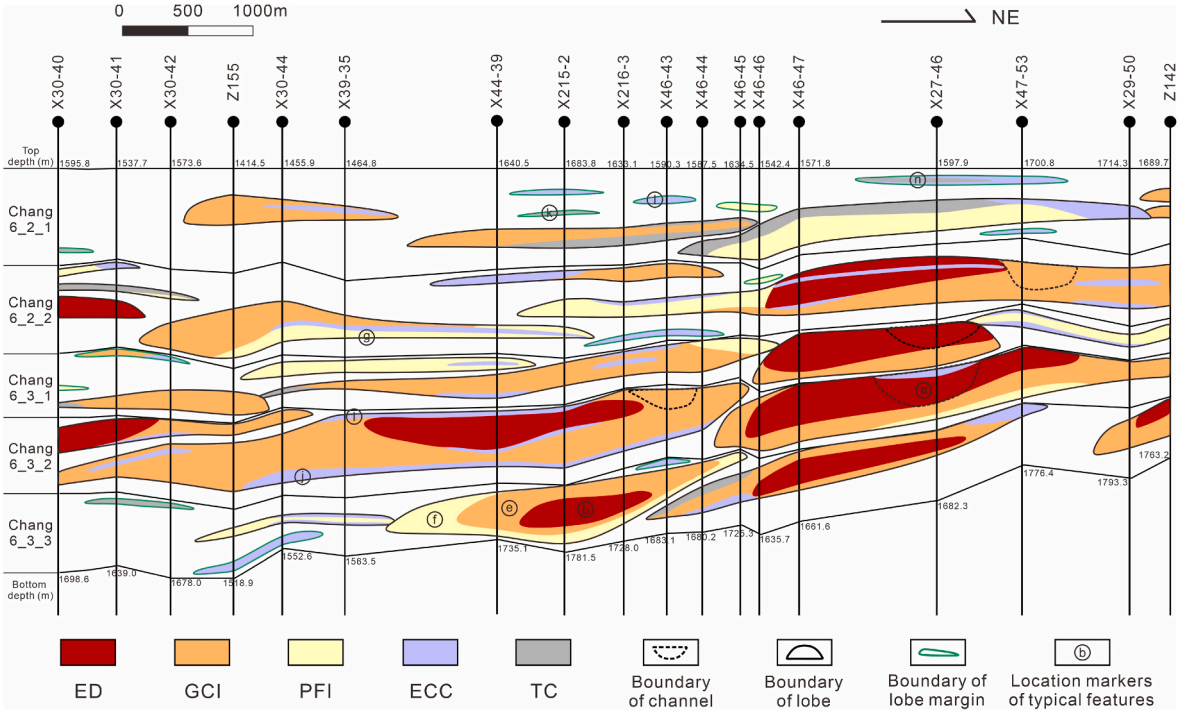

Fig. 10. Profile distribution of the diagenetic facies and sedimentary architecture parallel to the paleocurrent direction in the dense well pattern area of the Heshui area (see BB' in Fig. 1c for the section position).

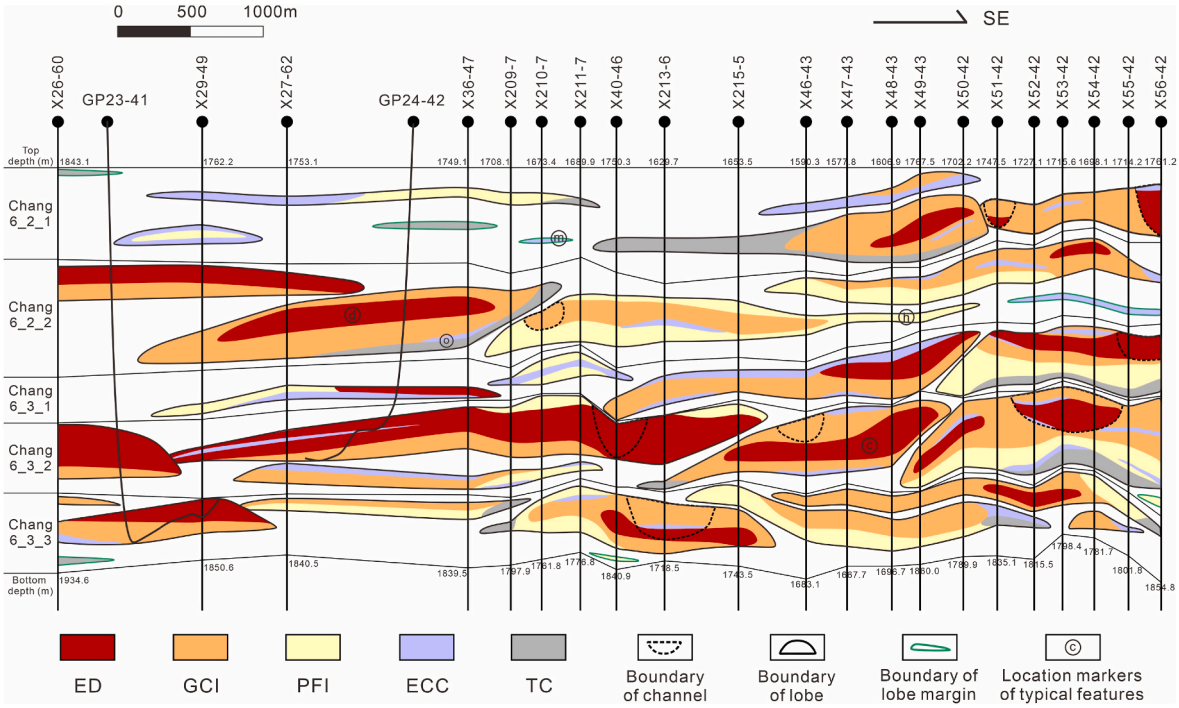

Fig. 11. Profile distribution of the diagenetic facies and sedimentary architecture perpendicular to the paleocurrent direction in the dense well pattern area of the Heshui area (see CC' in Fig. 1c for the section position).

pattern area (Fig. 1c). It is found that there are significant differences in lateral extent of different diagenetic facies in the tight sandstones (Table 2 and Fig. 9).

The maximum lateral extent of different diagenetic facies in the horizontal wells is shown in Table 2. The maximum lateral extent of ED diagenetic facies is up to approximately 720 m, suggesting that the actual maximum lateral extent of ED diagenetic facies may be greater than 720 m due to the limitations of the drilling length of horizontal wells. The maximum lateral extent of GCI and PFI diagenetic facies are smaller than that of ED diagenetic facies, about 420 m and 350 m, respectively. ECC and TC diagenetic facies have maximum lateral extents of less than 30 m and 160 m, respectively. This may be due to the relatively high drilling ratio of high-quality reservoirs for ED, GCI and PFI diagenetic facies in horizontal wells in the study area, while the ECC and TC diagenetic facies are rarely encountered in horizontal wells. That is, the type of diagenetic facies developed in the horizontal sections is related to the drilling ratio of high-quality sandstones. The above analyses show that the maximum lateral extent of diagenetic facies in the Chang 6 tight sandstones can be greater than 700 m or even less than 50 m, indicating that the distribution of diagenetic facies in the sublacustrine-fan tight sandstones is extremely complex.

5.1.2. Complex stacking patterns and geometries of diagenetic facies within the framework of sedimentary architecture correlation

The stacking patterns of diagenetic facies in the Chang 6 sandstones of the Heshui area were constructed within the framework of sedimentary architecture correlation of multiple wells. Variations of the five diagenetic facies in the Chang 6 sandstones depend on two sets of multi-layer correlation sections parallel and perpendicular to the paleocurrent direction in the dense well pattern area of the Heshui area. Various diagenetic facies exhibit a variety of geometric forms and are superimposed in varied styles (Figs. 10 and 11). Diagenetic facies appears to vary more rapidly perpendicular to the paleocurrent direction than that parallel to the paleocurrent direction, indicating more heterogeneity in the former (Figs. 10 and 11). The ED and GCI diagenetic facies are present across the study area, especially the GCI diagenetic facies. The ED diagenetic facies with relatively good reservoir quality are generally elongated or lenticular parallel or perpendicular to the paleocurrent, and are mostly found in the middle of the channel and lobe sandstones (ⓐ, ⓑ in Fig. 10 and ⓒ, ⓓ in Fig. 11). The GCI diagenetic facies is widely distributed in the lobe sand bodies, usually irregularly surrounding ED diagenetic facies (ⓔ in Fig. 10) or adjacent to PFI diagenetic facies (ⓕ in Fig. 10). The PFI diagenetic facies can usually be detected at the bottom of the lobe sandbodies (ⓖ in Fig. 10) or the lobe margin sandbodies (ⓗ in Fig. 11) in elongated shapes. The ECC and TC diagenetic facies typically occur as thin intervals near the sandstone-mudstone contacts (ⓘ, ⓙ in Fig. 10), or as isolated lenses that are recognizable in only one or two wells in the correlation sections (ⓚ, ⓛ in Fig. 10 and ⓜ in Fig. 11). Moreover, the ECC diagenetic facies is locally adjacent to TC diagenetic facies (ⓝ in Fig. 10 and ⓞ in Fig. 11),

Table 3
Scale variations of various diagenetic facies of the Chang 6 tight sandstones obtained from the integrated analysis of horizontal wells and development wells with small spacing in the dense well pattern area.

Diagenetic facies	Width perpendicular to the paleocurrent direction (m)		Length parallel to the paleocurrent direction (m)		Maximum thickness (m)	
	Main range of variation	Average	Main range of variation	Average	Main range of variation	Average
ED	400–4000	1500	600–4200	1600	2.0–11	5.0
GCI	400–2800	1800	500–5300	2500	2.0–13	7.5
PFI	500–3400	1200	300–3500	1500	1.5–7.0	3.0
ECC	200–2200	600	350–3600	1200	0.5–3.5	1.5
TC	150–2700	800	450–2500	1000	0.5–5.5	2.0

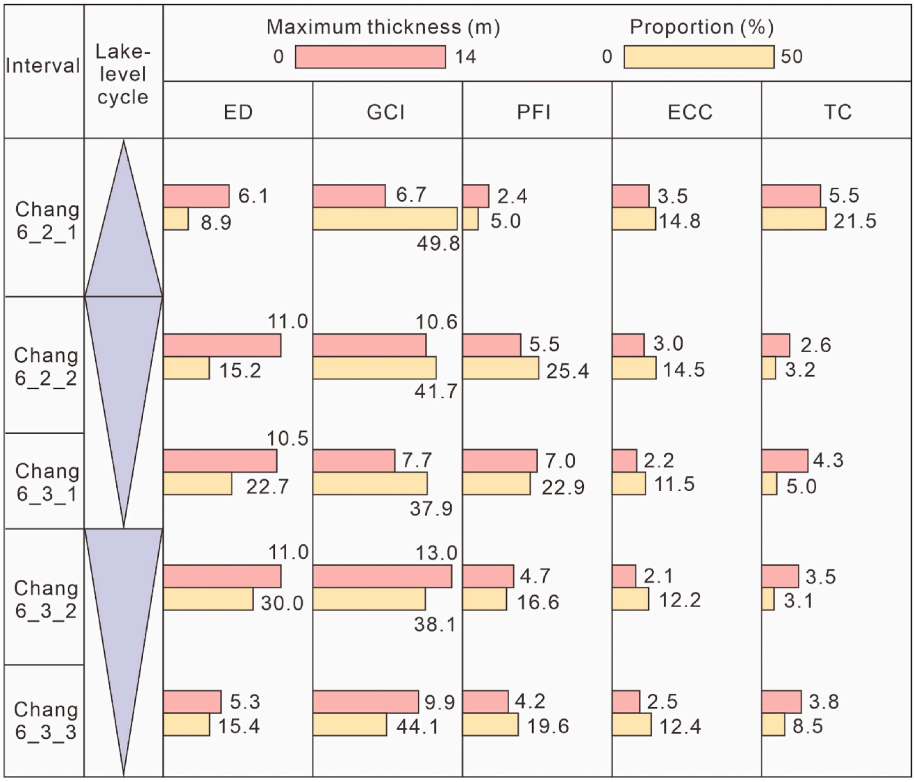

Fig. 12. Variations in the maximum thickness and proportion of various diagenetic facies associated with lake-level cycles in the Heshui area.

which may be due to the intense mechanical compaction of the TC diagenetic facies leading to fluid expulsion and thus facilitating the formation of abundant carbonate cements in the adjacent sandstone (Miocic et al., 2020). Irrespective of whether the diagenetic facies occur in different architectural units or different positions of the same architectural unit within the sublacustrine-fan deposits, the diagenetic facies always displays variations in stacking patterns (Figs. 10 and 11). But generally speaking, the various diagenetic facies from PFI to GCI to ED are typically superimposed sequentially within a complete lobe sand body from bottom to top, the TC diagenetic facies commonly occurs lateral to the PFI diagenetic facies at the margins of the lobe sand bodies, and the ECC diagenetic facies is generally randomly distributed on the top and bottom of the ED or GCI diagenetic facies and may overlap with TC diagenetic facies.

5.2. Quantitative scale of diagenetic facies for the Chang 6 tight sandstones

Based on the analyses of diagenetic facies distribution patterns in the Chang 6 tight sandstones in thin intervals, the quantitative scale variations of different diagenetic facies are summarized (Table 3), including the width perpendicular to the paleocurrent direction, the length parallel to the paleocurrent direction and the maximum thickness. The width and length extents of the GCI diagenetic facies are the largest, ranging from 400 m to 2800 m (average 1800 m) and 500 m–5300 m (average 2500 m), respectively. The average maximum thickness of the GCI diagenetic facies is approximately 7.5 m. The width and length extent of the ED diagenetic facies range from 400 m to 4000 m (average 1500 m) and 600 m–4200 m (average 1600 m), respectively, both of which are mostly less than that of the GCI diagenetic facies. Maximum thicknesses of both GCI and ED diagenetic facies can exceed 10 m. The PFI diagenetic facies has width and length extents of 500–3400 m and 300–3500 m, respectively. The length along the paleocurrent direction of the ECC diagenetic facies is locally greater than 3500 m, although the average maximum thickness is about 1.5 m, indicating that the length of the ECC diagenetic facies is weakly associated with its maximum thickness. For the TC diagenetic facies, the width and length extents are commonly less than 2700 m, and the maximum thickness is generally less than 5.5 m with an average of 2 m. On the whole, the GCI diagenetic facies has the largest width perpendicular to the paleocurrent direction, length along the paleocurrent direction and the maximum thickness, followed by the ED diagenetic facies (Table 3). From PFI, ED to GCI diagenetic facies, the average of width (1200 m, 1500 m–1800 m) and length (1500 m, 1600 m–2500 m) and the average of maximum thickness (3 m, 5 m to 7.5m) tend to increase. But for the same type of diagenetic facies, as illustrated in Figs. 10 and 11, the lateral extent is not significantly correlated with the maximum thickness, especially for the ECC diagenetic facies that can extend very far more than 3000 m with a thickness of less than 1.5 m (Table 3), demonstrating the extremely high variability and complexity of the distribution of tight sandstone diagenetic facies within sublacustrine-fan deposits.

5.3. Variations in thickness and proportion of various diagenetic facies associated with lake-level cycles

Based on the analysis of the relationship between the distribution of different diagenetic facies and the changes in lake-level in the Chang 6 interval, it is found that variations in thickness and proportion (i.e., the ratio of the thickness of a diagenetic facies to the total thickness of the interval) of diagenetic facies are closely related to lake-level changes (Fig. 12). The thin intervals of Chang 6_3_3 to Chang 6_2_1 from bottom to the top show lake level falling first and then rising (Qu et al., 2021). As shown in Fig. 12, from Chang 6_3_3 to Chang 6_3_2 and Chang 6_3_1 to Chang 6_2_2, the maximum thickness and proportion of the ED, GCI and PFI diagenetic facies generally exhibit a general increasing trend with the falling lake-level, whereas this relationship is opposite for the TC diagenetic facies. Furthermore, the maximum thickness and proportion of the ED, GCI and PFI diagenetic facies commonly show a decreasing trend with the rising lake-level from Chang 6_2_2 to Chang 6_2_1 (Fig. 12), whereas this relationship is opposite for the TC

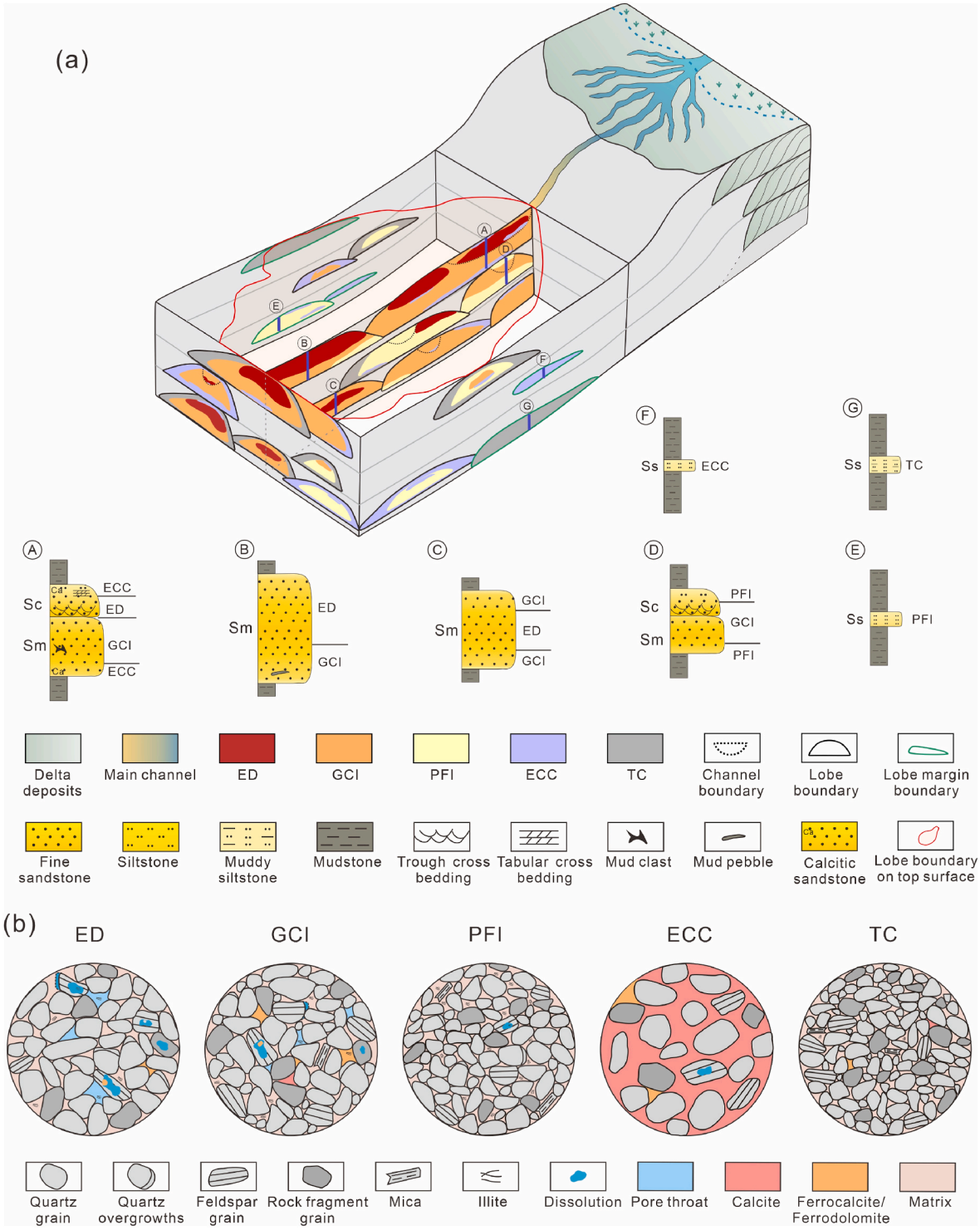

Fig. 13. Three-dimensional model showing the spatial variation in diagenetic facies of tight sandstones within sublacustrine-fan deposits. (a) Distribution of diagenetic facies among different sedimentary architectures and lithofacies associations in the sublacustrine-fan deposits; (b) Characteristics of diagenetic alterations and pore systems in different diagenetic facies. The descriptions of the diagenetic facies codes ED, GCI, PFI, ECC, TC and the lithofacies codes Sc, Sm, Ss are shown in Table 1.

diagenetic facies with relatively poor reservoir quality. However, the maximum thickness and proportion of the ECC diagenetic facies do not vary significantly with lake-level changes (Fig. 12), which may be due to the fact that carbonate cementation is significantly controlled by properties of the pore fluids and the adjacent mudstones in the deep-water gravity-flow deposits (Dutton, 2008; Yang et al., 2018; Wang et al., 2019; Civitelli et al., 2023).

5.4. Spatial variation model for diagenetic facies in tight sandstones from sublacustrine-fan deposits

By summarizing the distribution characteristics of diagenetic facies in the Chang 6 sandstones, a spatial variation model of diagenetic facies in tight sandstones within sublacustrine-fan deposits is proposed (Fig. 13). It can been seen there are significant differences in diagenetic

facies between different lithofacies, different architectural elements and different parts of the same architectural element (Ⓐ-Ⓖ in Fig. 13).

The GCI diagenetic facies is the most widely distributed facies in the sublacustrine-fan deposits, whereas the ECC and TC diagenetic facies are relatively few. The ED diagenetic facies with relatively good reservoir quality is mainly developed in the middle of channels and lobes, generally in the form of elongated lenses. The GCI and PFI diagenetic facies with relatively moderate reservoir quality are always distributed around the margins of ED diagenetic facies, mainly developing in the lobe main bodies or locally at the edges of channels. The TC diagenetic facies with relatively poor reservoir quality typically occurs along the margins of lobes in the form of isolated lenses or thin beds. The ECC diagenetic facies is commonly developed in fine-grained sandstones (Sc or Sm lithofacies) at the top and bottom of lobes and channels or in siltstone to very fine-grained sandstones (Ss lithofacies) at the margins of lobe sand bodies. Furthermore, the diagenetic facies and reservoir quality vary more significantly in the direction perpendicular to the paleocurrent than in the direction parallel to the paleocurrent. Overall, from the center to the edge of the channel and from the main body to margin of the lobe, sandstones of the ED and GCI diagenetic facies with relatively good reservoir quality gradually change to the sandstones of the ECC and TC diagenetic facies with relatively poor reservoir quality (Fig. 13), which is helpful for the prediction of high-quality reservoirs and the exploration and development of tight sandstone oil.

6. Conclusions

(1) Five diagenetic facies are recognized in the Chang 6 tight sandstones, including ED, GCI, PFI, ECC and TC diagenetic facies. The BP neural network method is used to build an identification model of diagenetic facies based on conventional well logs with an identification accuracy of 84.97%, and the blind test shows the high consistency of the predicted results with core analysis results.

(2) Diagenetic facies of tight sandstones within sublacustrine-fan deposits show extremely high variability and complexity in space. The GCI diagenetic facies is most widely distributed within lobe sand bodies as elongated lenses, usually irregularly surrounding the ED diagenetic facies or adjacent to the PFI diagenetic facies. The TC diagenetic facies is commonly found in lateral superposition with the PFI diagenetic facies at the margins of the lobe sand bodies, and the ECC diagenetic facies is generally randomly distributed in the form of thin beds on the top and bottom of the ED or GCI diagenetic facies and may overlap with the TC diagenetic facies.

(3) From the PFI, ED to GCI diagenetic facies, the average width perpendicular to the paleocurrent direction, the length parallel to the paleocurrent direction and the maximum thickness tend to increase. But for the same type of diagenetic facies, the lateral extent is not significantly correlated with the maximum thickness, especially for the ECC diagenetic facies that can extend laterally for more than 3000 m with a thickness of less than 1.5 m. In addition, variations in thickness and proportion of various diagenetic facies are closely associated with lake-level cycles.

Declaration of competing interest

The authors declare that they have no known competing financial interests or personal relationships that could have appeared to influence the work reported in this paper.

Data availability

The authors do not have permission to share data.

Acknowledgments

This study was financially supported by the National Natural Science Foundation of China (No. 42272186), the China Postdoctoral Science Foundation (No. 2022M723489), the Strategic Cooperation Technology Projects of CNPC and CUPB (No. ZLZX2020-02-02-02), and the Science Foundation of China University of Petroleum (Beijing) (No. 2462021XKBH010). The authors would also like to appreciate the Research Institute of Petroleum Exploration and Development of the PetroChina Changqing Oilfield Company for providing basic geological data.

References

Amendola, U., Perri, F., Critelli, S., Monaco, P., Cirilli, S., Trecci, T., Rettori, R., 2016. Composition and provenance of the Macigno formation (late Oligocene–early Miocene) in the Trasimeno lake area (northern Apennines). Mar. Petrol. Geol. 69, 146–167. https://doi.org/10.1016/J.MARPETGEO.2015.10.019.

Barbera, G., Critelli, S., Mazzoleni, P., 2011. Petrology and geochemistry of Cretaceous sedimentary rocks of the Monte Soro unit (Sicily, Italy): constraints on weathering, diagenesis, and provenance. J. Geol. 119, 51–68. https://doi.org/10.1086/657340.

Bell, D., Kane, I.A., Pontén, A.S.M., Flint, S.S., Hodgson, D.M., Barrett, B.J., 2018. Spatial variability in depositional reservoir quality of deep-water channel-fill and lobe deposits. Mar. Petrol. Geol. 98, 97–115. https://doi.org/10.1016/j.marpetgeo.2018.07.023.

Cao, J., Wang, X., Fan, L., Yuan, X., Wei, F., 2021. Deep water tight sandstone reservoir characteristics and diagenetic facies analysis: a case study of Chang 7 oil-bearing formation in Xifeng area, Ordos Basin, NW China. J. Northwest For. Univ. 51, 80–94. https://doi.org/10.16152/j.cnki.xdxbzr.2021-01-011 (in Chinese with English abstract).

Caracciolo, L., Arribas, J., Ingersoll, R.V., Critelli, S., 2015. The diagenetic destruction of porosity in plutoniclastic petrofacies: the Miocene Diligencia and Eocene Maniobra formations, Orocopia Mountains, southern California, USA. In: Scott, R.A., Smyth, H. R., Morton, A.C., Richardson, N. (Eds.), Sediment Provenance Studies in Hydrocarbon Exploration and Production, vol. 386. Geological Society, London, Special Publication, pp. 49–62. https://doi.org/10.1144/SP386.9.

Civitelli, M., Ravidà, D.C.G., Borrelli, M., Criniti, S., Falsetta, E., 2023. Diagenesis and petrophysics of Miocene sandstones within southern Apennines foreland, Italy. Mar. Petrol. Geol. 155, 106411 https://doi.org/10.1016/J.MARPETGEO.2023.106411.

Critelli, S., Perri, F., Arribas, J., Herrero, M.J., 2018. Sandstone detrital modes and diagenetic evolution of Mesozoic continental red beds from western-central circum-Mediterranean orogenic belts. In: Ingersoll, R.V., Lawton, T.F., Graham, S. (Eds.), Tectonics, Sedimentary Basins, and Provenance: A Celebration of the Career of William R. Dickinson, vol. 540. Geological Society of America Special Paper, pp. 119–132. https://doi.org/10.1130/2018.2540(06.

Cui, Y., Wang, G., Jones, S.J., Zhou, Z., Ran, Y., Lai, J., Li, R., Deng, L., 2017. Prediction of diagenetic facies using well logs – a case study from the upper Triassic Yanchang Formation, Ordos Basin, China. Mar. Petrol. Geol. 81, 50–65. https://doi.org/10.1016/J.MARPETGEO.2017.01.001.

Desbois, G., Urai, J.L., Kukla, P.A., Konstanty, J., Baerle, C., 2011. High-resolution 3D fabric and porosity model in a tight gas sandstone reservoir:A new approach to investigate microstructures from mm- to nm-scale combining argon beam cross-sectioning and SEM imaging. J. Pet. Sci. Eng. 78, 243–257. https://doi.org/10.1016/J.PETROL.2011.06.004.

Dill, H.G., Khishigsuren, S., Melcher, F., Bulgamaa, J., Bolorma, K., Botz, R., Schwarz-Schampera, U., 2005. Facies-related diagenetic alteration in lacustrine-deltaic red beds of the Paleogene Ergeliin Zoo formation (Erdene Sum area, S. Gobi, Mongolia). Sediment. Geol. 181, 1–24. https://doi.org/10.1016/J.SEDGEO.2005.06.007.

Dutton, S.P., 2008. Calcite cement in Permian deep-water sandstones, Delaware Basin, west Texas: Origin, distribution, and effect on reservoir properties. Am. Assoc. Petrol. Geol. Bull. 92, 765–787. https://doi.org/10.1306/01280807107.

El-ghali, M.A.K., Mansurbeg, H., Morad, S., Al-Aasm, I., Ajdanlisky, G., 2006. Distribution of diagenetic alterations in fluvial and paralic deposits within sequence stratigraphic framework: Evidence from the Petrohan Terrigenous group and the Svidol formation, lower Triassic, NW Bulgaria. Sediment. Geol. 190, 299–321. https://doi.org/10.1016/J.SEDGEO.2006.05.021.

Friesen, O.J., Dashtgard, S.E., Miller, J., Schmitt, L., Baldwin, C., 2017. Permeability heterogeneity in bioturbated sediments and implications for waterflooding of tight-oil reservoirs, Cardium Formation, Pembina Field, Alberta, Canada. Mar. Petrol. Geol. 82, 371–387. https://doi.org/10.1016/J.MARPETGEO.2017.01.019.

Fu, J., Wu, S., Fu, J., Hu, L., Zhang, H., Liu, X., 2013. Research on quantitative diagenetic facies of the Yanchang Formation in Longdong area, Ordos Basin. Earth Sci. Front. 20, 86–97 (in Chinese with English abstract).

Ghanizadeh, A., Clarkson, C.R., Aquino, S., Ardakani, O.H., Sanei, H., 2015. Petrophysical and geomechanical characteristics of Canadian tight oil and liquid-rich gas reservoirs: I. Pore network and permeability characterization. Fuel 153, 664–681. https://doi.org/10.1016/j.fuel.2015.03.020.

Gogoi, T., Chatterjee, R., 2019. Estimation of petrophysical parameters using seismic inversion and neural network modeling in Upper Assam basin, India. Geosci. Front. 10, 1113–1124. https://doi.org/10.1016/J.GSF.2018.07.002.

Hart, B.S., 2006. Seismic expression of fracture-swarm sweet spots, Upper Cretaceous tight-gas reservoirs, San Juan Basin. Am. Assoc. Petrol. Geol. Bull. 90, 1519–1534. https://doi.org/10.1306/05020605171.

Higgs, K.E., Crouch, E.M., Raine, J.I., 2017. An interdisciplinary approach to reservoir characterisation; an example from the early to middle Eocene Kaimiro Formation, Taranaki Basin, New Zealand. Mar. Petrol. Geol. 86, 111–139. https://doi.org/10.1016/j.marpetgeo.2017.05.018.

Higgs, K.E., Zwingmann, H., Reyes, A.G., Funnell, R.H., 2007. Diagenesis, porosity evolution, and petroleum emplacement in tight gas reservoirs, Taranaki Basin, New Zealand. J. Sediment. Res. 77, 1003–1025. https://doi.org/10.2110/jsr.2007.095.

Jiang, M., Fang, H., Liu, Y., Zhang, Y., Wang, C., 2023. On movable fluid saturation of tight sandstone and main controlling factors —case study on the Fuyu oil layer in the Da'an oilfield in the Songliao basin. Energy 267, 126476. https://doi.org/10.1016/j.energy.2022.126476.

Kadkhodaie, R., Kadkhodaie, A., Rezaee, R., 2021. Study of pore system properties of tight gas sandstones based on analysis of the seismically derived velocity deviation log: a case study from the Perth Basin of western Australia. J. Pet. Sci. Eng. 196, 108077 https://doi.org/10.1016/J.PETROL.2020.108077.

La Croix, A.D., Gingras, M.K., Pemberton, S.G., Mendoza, C.A., MacEachern, J.A., Lemiski, R.T., 2013. Biogenically enhanced reservoir properties in the Medicine Hat gas field, Alberta, Canada. Mar. Petrol. Geol. 43, 464–477. https://doi.org/10.1016/J.MARPETGEO.2012.12.002.

Lai, J., Fan, X., Liu, B., Pang, X., Zhu, S., Xie, W., Wang, G., 2020. Qualitative and quantitative prediction of diagenetic facies via well logs. Mar. Petrol. Geol. 120, 104486 https://doi.org/10.1016/J.MARPETGEO.2020.104486.

Lai, J., Wang, G., Ran, Y., Zhou, Z., Cui, Y., 2016. Impact of diagenesis on the reservoir quality of tight oil sandstones: the case of Upper Triassic Yanchang Formation Chang 7 oil layers in Ordos Basin, China. J. Pet. Sci. Eng. 145, 54–65. https://doi.org/10.1016/j.petrol.2016.03.009.

Lai, J., Wang, G., Wang, S., Cao, J., Li, M., Pang, X., Zhou, Z., Fan, X., Dai, Q., Yang, L., He, Z., Qin, Z., 2018. Review of diagenetic facies in tight sandstones: diagenesis, diagenetic minerals, and prediction via well logs. Earth Sci. Rev. 185, 234–258. https://doi.org/10.1016/j.earscirev.2018.06.009.

Law, B.E., 2002. Basin-centered gas systems. Am. Assoc. Petrol. Geol. Bull. 86, 1891–1919. https://doi.org/10.1306/61EEDDB4-173E-11D7-8645000102C1865D.

Li, G., Lei, Z., Dong, W., Wang, H., Zheng, X., Tan, J., 2022a. Progress, challenges and prospects of unconventional oil and gas development of CNPC. China Pet. Explor. 27, 1–11. https://doi.org/10.3969/j.issn.1672-7703.2022.01.001 (in Chinese with English abstract).

Li, M., Zhang, Liqiang, Li, Z., Zhang, Liang, Mao, L., Xu, X., 2021. Diagenetic facies division and logging identification of tight sandstone in the lower conglomerate member of lower Jurassic Ahe Formation in Tarim basin: case study of Yiqikelike area in Kuqa depression. Nat. Gas Geosci. 32, 1559–1570. https://doi.org/10.11764/j.issn.1672-1926.2021.03.001 (in Chinese with English abstract).

Li, Y., Chang, X., Yin, W., Wang, G., Zhang, Jinliang, Shi, B., Zhang, Jianhua, Mao, L., 2019. Quantitative identification of diagenetic facies and controls on reservoir quality for tight sandstones: a case study of the Triassic Chang 9 oil layer, Zhenjing area, Ordos Basin. Mar. Petrol. Geol. 102, 680–694. https://doi.org/10.1016/j.marpetgeo.2019.01.025.

Li, Z., Wu, S., Xia, D., Zhang, X., Huang, M., 2017. Diagenetic alterations and reservoir heterogeneity within the depositional facies: a case study from distributary-channel belt sandstone of Upper Triassic Yanchang Formation reservoirs (Ordos Basin, China). Mar. Petrol. Geol. 86, 950–971. https://doi.org/10.1016/j.marpetgeo.2017.07.002.

Li, Z., Zhang, Liqiang, Yuan, W., Chen, X., Zhang, Liang, Li, M., 2022b. Logging identification for diagenetic facies of tight sandstone reservoirs: a case study in the lower Jurassic Ahe formation, Kuqa depression of Tarim basin. Mar. Petrol. Geol. 139, 105601 https://doi.org/10.1016/J.MARPETGEO.2022.105601.

Liu, E., Wang, H., Feng, Y., Pan, S., Jing, Z., Ma, Q., Gan, H., Zhao, J. xin, 2020. Sedimentary architecture and provenance analysis of a sublacustrine fan system in a half-graben rift depression of the South China Sea. Sediment. Geol. 409, 105781 https://doi.org/10.1016/J.SEDGEO.2020.105781.

Liu, J., Xian, B., Wang, J., Ji, Y., Lu, Z., Liu, S., 2017. Sedimentary architecture of a sub-lacustrine debris fan: Eocene Dongying depression, Bohai Bay Basin, east China. Sediment. Geol. 362, 66–82. https://doi.org/10.1016/j.sedgeo.2017.09.014.

Lu, H., Li, Q., Yue, D., Wu, S., Fu, Y., Tang, R., Zhang, Z., 2021. Study on optimal selection of porosity logging interpretation methods for Chang 73 segment of the Yanchang Formation in the southwestern Ordos Basin, China. J. Pet. Sci. Eng. 198, 108153 https://doi.org/10.1016/j.petrol.2020.108153.

Ma, B., Yang, S., Zhang, H., Kong, Q., Song, C., Wang, Y., Bai, Q., Wang, X., 2018. Diagenetic facies quantitative evaluation of low-permeability sandstone: a case study on Chang 8^2 reservoirs in the Zhenbei area, Ordos basin. Energy Explor. Exploit. 36, 414–432. https://doi.org/10.1177/0144598717738813.

Ma, Y.Z., Moore, W.R., Gomez, E., Clark, W.J., Zhang, Y., 2016. Tight gas sandstone reservoirs, Part 1: Overview and lithofacies. Unconv. Oil Gas Resour. Handb. Eval. Dev. 405–427. https://doi.org/10.1016/B978-0-12-802238-2.00014-6.

Masters, J.A., 1979. Deep Basin gas Trap, western Canada. Am. Assoc. Petrol. Geol. Bull. 63, 152–181. https://doi.org/10.1306/c1ea55cb-16c9-11d7-8645000102c1865d.

Miocic, J.M., Girard, J.P., Schöner, R., Gaupp, R., 2020. Mudstone/sandstone ratio control on carbonate cementation and reservoir quality in Upper Permian Rotliegend sandstones, offshore The Netherlands. Mar. Petrol. Geol. 115, 104293 https://doi.org/10.1016/J.MARPETGEO.2020.104293.

Morad, S., Al-ramadan, K., Ketzer, J.M., De Ros, L.F., 2010. The impact of diagenesis on the heterogeneity of sandstone reservoirs: a review of the role of depositional facies and sequence stratigraphy. Am. Assoc. Petrol. Geol. Bull. 94, 1267–1309. https://doi.org/10.1306/04211009178.

Morad, S., Ketzer, J.M., De Ros, L.F., 2000. Spatial and temporal distribution of diagenetic alterations in siliciclastic rocks: implications for mass transfer in sedimentary basins. Sedimentology 47 (Suppl. 1), 95–120. https://doi.org/10.1046/j.1365-3091.2000.00007.x.

Nguyen, B.T.T., Jones, S.J., Goulty, N.R., Middleton, A.J., Grant, N., Ferguson, A., Bowen, L., 2013. The role of fluid pressure and diagenetic cements for porosity preservation in Triassic fluvial reservoirs of the Central Graben, North Sea. Am. Assoc. Petrol. Geol. Bull. 97, 1273–1302. https://doi.org/10.1306/01151311163.

Ortiz-Orduz, A., Ríos-Reyes, C.A., Vargas-Escudero, M.A., García-González, M., 2021. Impact of diagenesis on the reservoir rock quality of the Cachiri Group tight sandstones in Cesar sub basin (Colombia): a case of study from ANH-CR-MONTECARLO 1X well. J. Nat. Gas Sci. Eng. 95, 104138 https://doi.org/10.1016/J.JNGSE.2021.104138.

Ozkan, A., Cumella, S.P., Milliken, K.L., Laubach, S.E., 2011. Prediction of lithofacies and reservoir quality using well logs, late Cretaceous Williams Fork formation, Mamm Creek field, Piceance basin, Colorado. Am. Assoc. Petrol. Geol. Bull. 95, 1699–1724. https://doi.org/10.1306/01191109143.

Qiu, Y., Meng, Q., Li, T., Zhang, L., 2001. The feasibility analysis of neural network in the prediction of lithology and lithofacies. Prog. Geophys. 16, 76–84 (in Chinese with English abstract).

Qu, X., Wang, W., Xie, Q., Yue, D., Liu, J., Wu, S., Zhang, X., Hu, J., 2021. Single Sandbody architecture of sublacustrine fan in a depression lacustrine BaSin-insights from Triassic Chang-6 oil-bearing interval in Heshui area of Ordos Basin, China. J. Earth Sci. Environ. 43, 850–867. https://doi.org/10.19814/j.jese.2020.10041.

Ran, Y., Wang, G., Lai, J., Zhou, Z., Cui, Y., Dai, Q., Chen, J., Wang, S., 2016. Quantitative characterization of diagenetic facies of tight sandstone oil reservoir by using logging Crossplot: a case study on Chang 7 tight sandstone oil reservoir in Huachi area, Ordos Basin. Acta Sedimentol. Sin. 34, 694–706. https://doi.org/10.14027/j.cnki.cjxb.2016.04.010 (in Chinese with English abstract).

Salim, A.M.A., Negash, B.M., Alansari, A.M.A., 2017. A diagenetic facies model for characterizing Yanan formation, Ordos Basin, north Central China. In: Proceedings of the International Conference on Integrated Petroleum Engineering and Geosciences (ICIPEG). Springer Nature Singapore Pte. Ltd. https://doi.org/10.1007/978-981-10-3650-7_23.

Stevenson, C.J., Peakall, J., 2010. Effects of topography on lofting gravity flows: implications for the deposition of deep-water massive sands. Mar. Petrol. Geol. 27, 1366–1378. https://doi.org/10.1016/j.marpetgeo.2010.03.010.

Wang, C., Wang, Q., Chen, G., He, L., Xu, Y., Chen, L., Chen, D., 2017b. Petrographic and geochemical characteristics of the lacustrine black shales from the Upper Triassic Yanchang Formation of the Ordos Basin, China: implications for the organic matter accumulation. Mar. Petrol. Geol. 86, 52–65. https://doi.org/10.1016/j.marpetgeo.2017.05.016.

Wang, J., Cao, Y., Liu, K., Liu, J., Kashif, M., 2017a. Identification of sedimentary-diagenetic facies and reservoir porosity and permeability prediction: an example from the Eocene beach-bar sandstone in the Dongying Depression, China. Mar. Petrol. Geol. 82, 69–84. https://doi.org/10.1016/J.MARPETGEO.2017.02.004.

Wang, W., Lin, C., Zhang, X., Dong, C., Ren, L., Lin, J., 2022a. Discussion of seismic diagenetic facies of deep reservoir in the East China Sea Basin. J. Pet. Sci. Eng. 208, 109352 https://doi.org/10.1016/j.petrol.2021.109352.

Wang, W., Lin, C., Zhang, X., Dong, C., Ren, L., Lin, J., 2022b. Seismic diagenetic facies prediction of tight sandstone in the offshore sparse well area: an example from the Xihu Depression of the East China Sea Basin. J. Pet. Sci. Eng. 216, 110825 https://doi.org/10.1016/J.PETROL.2022.110825.

Wang, W., Yue, D., Eriksson, K.A., Liu, X., Liang, X., Qu, X., Xie, Q., 2020a. Qualitative and quantitative characterization of multiple factors that influence movable fluid saturation in lacustrine deep-water gravity-flow tight sandstones from the Yanchang Formation, southern Ordos Basin, China. Mar. Petrol. Geol. 121, 104625 https://doi.org/10.1016/j.marpetgeo.2020.104625.

Wang, W., Yue, D., Eriksson, K.A., Qu, X., Li, W., Lv, M., Zhang, J., Zhang, X., 2020b. Quantification and prediction of pore structures in tight oil reservoirs based on Multifractal Dimensions from integrated pressure- and rate-controlled porosimetry for the upper Triassic Yanchang Formation, Ordos Basin, China. Energy Fuels 34, 4366–4383. https://doi.org/10.1021/acs.energyfuels.0c00178.

Wang, W., Yue, D., Zhao, J., Li, W., Wang, B., Wu, S., Li, S., 2019. Diagenetic alteration and its control on reservoir quality of tight sandstones in lacustrine deep-water gravity-flow deposits : a case study of the Yanchang Formation , southern Ordos Basin , China. Mar. Petrol. Geol. 110, 676–694. https://doi.org/10.1016/j.marpetgeo.2019.07.046.

Wang, X., Shi, F., Yu, L., Li, Y., 2013. MATLAB Neural Network Analysis of 43 Cases. Beijing University of Aeronautics and Astronautics Press, Beijing, pp. 11–19 (in Chinese).

Wang, Y., Lu, Y., 2021. Diagenetic facies prediction using a LDA-assisted SSOM method for the Eocene beach-bar sandstones of Dongying Depression, East China. J. Pet. Sci. Eng. 196, 108040 https://doi.org/10.1016/J.PETROL.2020.108040.

Wu, D., Liu, S., Chen, H., Lin, L., Yu, Y., Xu, C., Pan, B., 2020. Investigation and prediction of diagenetic facies using well logs in tight gas reservoirs: Evidences from the Xu-2 member in the Xinchang structural belt of the western Sichuan Basin, western China. J. Pet. Sci. Eng. 192, 107326 https://doi.org/10.1016/J.PETROL.2020.107326.

Wu, S., 2010. Reservoir Characterization and Modeling. Petroleum Industry Press, Beijing (in Chinese).

Xi, K., Cao, Y., Jahren, J., Zhu, R., Bjørlykke, K., Haile, B.G., Zheng, L., Hellevang, H., 2015. Diagenesis and reservoir quality of the lower Cretaceous Quantou formation tight sandstones in the southern Songliao Basin, China. Sediment. Geol. 330, 90–107. https://doi.org/10.1016/j.sedgeo.2015.10.007.

Yang, J., 2002. Tectonic Evolution and Oil-Gas Reservoirs Distribution in Ordos Basin. Petroleum Industry Press, Beijing, pp. 1–37 (in Chinese).

Yang, R., He, Z., Qiu, G., Jin, Z., Sun, D., Jin, X., 2014. A Late Triassic gravity flow depositional system in the southern Ordos Basin. Petrol. Explor. Dev. 41, 724–733. https://doi.org/10.1016/S1876-3804(14)60086-0.

Yang, T., Cao, Y., Friis, H., Liu, K., Wang, Y., Zhou, L., Zhang, S., Zhang, H., 2018. Genesis and distribution pattern of carbonate cements in lacustrine deep-water gravity-flow sandstone reservoirs in the third member of the Shahejie Formation in the Dongying Sag, Jiyang Depression, Eastern China. Mar. Petrol. Geol. 92, 547–564. https://doi.org/10.1016/j.marpetgeo.2017.11.020.

Yao, J., Zhao, Y., Liu, G., Qi, Y., Li, Y., Luo, A., Zhang, X., 2018. Formation patterns of Chang 9 oil reservoir in Triassic Yanchang Formation, Ordos Basin, NW China. Petrol. Explor. Dev. 45, 389–401. https://doi.org/10.1016/S1876-3804(18)30044-2.

Yu, J., Luo, G., Li, B., Pan, T., Yu, H., Kuang, H., Chu, X., Zhang, X., 2022. Diagenesis and diagenetic facies of upper Wuerhe Formation in the Shawan Sag. Geosci. 36, 1095–1104. https://doi.org/10.19657/j.geoscience.1000-8527.2022.206 (in Chinese with English abstract).

Yue, D., Wu, S., Xu, Z., Xiong, L., Chen, D., Ji, Y., Zhou, Y., 2018. Reservoir quality, natural fractures, and gas productivity of upper Triassic Xujiahe tight gas sandstones in western Sichuan Basin, China. Mar. Petrol. Geol. 89, 370–386. https://doi.org/10.1016/j.marpetgeo.2017.10.007.

Zeng, H., Zhao, W., Xu, Z., Fu, Q., Hu, S., Wang, Z., Li, B., 2018. Carbonate seismic sedimentology: a case study of Cambrian Longwangmiao formation, gaoshiti-Moxi area, Sichuan Basin, China. Petrol. Explor. Dev. 45, 830–839. https://doi.org/10.1016/S1876-3804(18)30086-7.

Zhang, W., Xiao, X., Miao, Q., Luo, J., Yu, W., Xu, Z., 2019. Main controlling factor of high quality reservoir and prediction of strong dissolution area in Huagang Formation, north-central Xihu Sag, East China Sea. J. Chengdu Univ. Technol. (Sci. Technol. Ed.) 46, 597–607. https://doi.org/10.3969/j.issn.1671-9727.2019.05.10 (in Chinese with English abstract).

Zhang, X., Zhang, T., Ju, C., Lin, C., Dong, C., Lin, J., Han, S., 2018. A Quantitative Method and Workflow for Diagenetic Facies Prediction of Tight Reservoir Based on Multiple Scale Information. China Patent. ZL201510895321.7.

Zhao, C., Jiang, Y., Wang, L., 2022. Data-driven diagenetic facies classification and well-logging identification based on machine learning methods: a case study on Xujiahe tight sandstone in Sichuan Basin. J. Pet. Sci. Eng. 217, 110798 https://doi.org/10.1016/J.PETROL.2022.110798.

Zhu, R., Zou, C., Mao, Z., Yang, H., Hui, X., Wu, S., Cui, J., Su, L., Li, S., Yang, Z., 2019. Characteristics and distribution of continental tight oil in China. J. Asian Earth Sci. 178, 37–51. https://doi.org/10.1016/J.JSEAES.2018.07.020.

Zhu, X., Dong, Y., Zeng, H., Lin, C., Zhang, X., 2020. Research status and thoughts on the development of seismic sedimentology in China. J. Palaeogeogr. 22, 397–411. https://doi.org/10.7605/gdlxb.2020.03.027 (in Chinese with English abstract).

Zou, C., Tao, S., Zhou, H., Zhang, X., He, D., Zhou, C., Wang, L., Wang, X., Li, F., Zhu, R., Luo, P., Yuan, X., Xu, C., Yang, H., 2008. Genesis, classification, and evaluation method of diagenetic facies. Petrol. Explor. Dev. 35, 526–540. https://doi.org/10.1016/S1876-3804(09)60086-0.

Zou, C., Zhu, R., Liu, K., Su, L., Bai, B., Zhang, X., Yuan, X., Wang, J., 2012. Tight gas sandstone reservoirs in China: characteristics and recognition criteria. J. Pet. Sci. Eng. 88–89, 82–91. https://doi.org/10.1016/j.petrol.2012.02.001.